12-1-1999

Measurement of the $B^0\bar{B}^0$ oscillation frequency using ℓD^{*+} pairs and lepton flavor tags

T. Affolder
Ernest Orlando Lawrence Berkeley National Laboratory, Berkeley, California

Kenneth A. Bloom
University of Nebraska-Lincoln, kenbloom@unl.edu

Collider Detector at Fermilab Collaboration

Measurement of the $B^0\bar{B}^0$ oscillation frequency using l^-D^{*+} pairs and lepton flavor tags

T. Affolder,[21] H. Akimoto,[42] A. Akopian,[35] M. G. Albrow,[10] P. Amaral,[7] S. R. Amendolia,[31] D. Amidei,[24] J. Antos,[1] G. Apollinari,[35] T. Arisawa,[42] T. Asakawa,[40] W. Ashmanskas,[7] M. Atac,[10] P. Azzi-Bacchetta,[29] N. Bacchetta,[29] M. W. Bailey,[26] S. Bailey,[14] P. de Barbaro,[34] A. Barbaro-Galtieri,[21] V. E. Barnes,[33] B. A. Barnett,[17] M. Barone,[12] G. Bauer,[22] F. Bedeschi,[31] S. Belforte,[39] G. Bellettini,[31] J. Bellinger,[43] D. Benjamin,[9] J. Bensinger,[4] A. Beretvas,[10] J. P. Berge,[10] J. Berryhill,[7] S. Bertolucci,[12] B. Bevensee,[30] A. Bhatti,[35] C. Bigongiari,[31] M. Binkley,[10] D. Bisello,[29] R. E. Blair,[2] C. Blocker,[4] K. Bloom,[24] S. Blusk,[34] A. Bocci,[31] A. Bodek,[34] W. Bokhari,[30] G. Bolla,[33] Y. Bonushkin,[5] D. Bortoletto,[33] J. Boudreau,[32] A. Brandl,[26] S. van den Brink,[17] C. Bromberg,[25] N. Bruner,[26] E. Buckley-Geer,[10] J. Budagov,[8] H. S. Budd,[34] K. Burkett,[14] G. Busetto,[29] A. Byon-Wagner,[10] K. L. Byrum,[2] M. Campbell,[24] A. Caner,[31] W. Carithers,[21] J. Carlson,[24] D. Carlsmith,[43] J. Cassada,[34] A. Castro,[29] D. Cauz,[39] A. Cerri,[31] P. S. Chang,[1] P. T. Chang,[1] J. Chapman,[24] C. Chen,[30] Y. C. Chen,[1] M. -T. Cheng,[1] M. Chertok,[37] G. Chiarelli,[31] I. Chirikov-Zorin,[8] G. Chlachidze,[8] F. Chlebana,[10] L. Christofek,[16] M. L. Chu,[1] S. Cihangir,[10] C. I. Ciobanu,[27] A. G. Clark,[13] M. Cobal,[31] E. Cocca,[31] A. Connolly,[21] J. Conway,[36] J. Cooper,[10] M. Cordelli,[12] J. Guimaraes da Costa,[24] D. Costanzo,[31] D. Cronin-Hennessy,[9] R. Cropp,[23] R. Culbertson,[7] D. Dagenhart,[41] F. DeJongh,[10] S. Dell'Agnello,[12] M. Dell'Orso,[31] R. Demina,[10] L. Demortier,[35] M. Deninno,[3] P. F. Derwent,[10] T. Devlin,[36] J. R. Dittmann,[10] S. Donati,[31] J. Done,[37] T. Dorigo,[14] N. Eddy,[16] K. Einsweiler,[21] J. E. Elias,[10] E. Engels, Jr.,[32] W. Erdmann,[10] D. Errede,[16] S. Errede,[16] Q. Fan,[34] R. G. Feild,[44] C. Ferretti,[31] I. Fiori,[3] B. Flaugher,[10] G. W. Foster,[10] M. Franklin,[14] J. Freeman,[10] J. Friedman,[22] Y. Fukui,[20] S. Gadomski,[23] S. Galeotti,[31] M. Gallinaro,[35] T. Gao,[30] M. Garcia-Sciveres,[21] A. F. Garfinkel,[33] P. Gatti,[29] C. Gay,[44] S. Geer,[10] D. W. Gerdes,[24] P. Giannetti,[31] P. Giromini,[12] V. Glagolev,[8] M. Gold,[26] J. Goldstein,[10] A. Gordon,[14] A. T. Goshaw,[9] Y. Gotra,[32] K. Goulianos,[35] H. Grassmann,[39] C. Green,[33] L. Groer,[36] C. Grosso-Pilcher,[7] M. Guenther,[33] G. Guillian,[24] R. S. Guo,[1] C. Haber,[21] E. Hafen,[22] S. R. Hahn,[10] C. Hall,[14] T. Handa,[15] R. Handler,[43] W. Hao,[38] F. Happacher,[12] K. Hara,[40] A. D. Hardman,[33] R. M. Harris,[10] F. Hartmann,[18] K. Hatakeyama,[35] J. Hauser,[5] J. Heinrich,[30] A. Heiss,[18] B. Hinrichsen,[23] K. D. Hoffman,[33] C. Holck,[30] R. Hollebeek,[30] L. Holloway,[16] R. Hughes,[27] J. Huston,[25] J. Huth,[14] H. Ikeda,[40] M. Incagli,[31] J. Incandela,[10] G. Introzzi,[31] J. Iwai,[42] Y. Iwata,[15] E. James,[24] H. Jensen,[10] M. Jones,[30] U. Joshi,[10] H. Kambara,[13] T. Kamon,[37] T. Kaneko,[40] K. Karr,[41] H. Kasha,[44] Y. Kato,[28] T. A. Keaffaber,[33] K. Kelley,[22] M. Kelly,[24] R. D. Kennedy,[10] R. Kephart,[10] D. Khazins,[9] T. Kikuchi,[40] M. Kirk,[4] B. J. Kim,[19] H. S. Kim,[23] S. H. Kim,[40] Y. K. Kim,[21] L. Kirsch,[4] S. Klimenko,[11] D. Knoblauch,[18] P. Koehn,[27] A. Köngeter,[18] K. Kondo,[42] J. Konigsberg,[11] K. Kordas,[23] A. Korytov,[11] E. Kovacs,[2] J. Kroll,[30] M. Kruse,[34] S. E. Kuhlmann,[2] K. Kurino,[15] T. Kuwabara,[40] A. T. Laasanen,[33] N. Lai,[7] S. Lami,[35] S. Lammel,[10] J. I. Lamoureux,[4] M. Lancaster,[21] G. Latino,[31] T. LeCompte,[2] A. M. Lee IV,[9] S. Leone,[31] J. D. Lewis,[10] M. Lindgren,[5] T. M. Liss,[16] J. B. Liu,[34] Y. C. Liu,[1] N. Lockyer,[30] M. Loreti,[29] D. Lucchesi,[29] P. Lukens,[10] S. Lusin,[43] J. Lys,[21] R. Madrak,[14] K. Maeshima,[10] P. Maksimovic,[14] L. Malferrari,[3] M. Mangano,[31] M. Mariotti,[29] G. Martignon,[29] A. Martin,[44] J. A. J. Matthews,[26] P. Mazzanti,[3] K. S. McFarland,[34] P. McIntyre,[37] E. McKigney,[30] M. Menguzzato,[29] A. Menzione,[31] E. Meschi,[31] C. Mesropian,[35] C. Miao,[24] T. Miao,[10] R. Miller,[25] J. S. Miller,[24] H. Minato,[40] S. Miscetti,[12] M. Mishina,[20] N. Moggi,[31] E. Moore,[26] R. Moore,[24] Y. Morita,[20] A. Mukherjee,[10] T. Muller,[18] A. Munar,[31] P. Murat,[31] S. Murgia,[25] M. Musy,[39] J. Nachtman,[5] S. Nahn,[44] H. Nakada,[40] T. Nakaya,[7] I. Nakano,[15] C. Nelson,[10] D. Neuberger,[18] C. Newman-Holmes,[10] C.-Y. P. Ngan,[22] P. Nicolaidi,[39] H. Niu,[4] L. Nodulman,[2] A. Nomerotski,[11] S. H. Oh,[9] T. Ohmoto,[15] T. Ohsugi,[15] R. Oishi,[40] T. Okusawa,[28] J. Olsen,[43] C. Pagliarone,[31] F. Palmonari,[31] R. Paoletti,[31] V. Papadimitriou,[38] S. P. Pappas,[44] A. Parri,[12] D. Partos,[4] J. Patrick,[10] G. Pauletta,[39] M. Paulini,[21] A. Perazzo,[31] L. Pescara,[29] T. J. Phillips,[9] G. Piacentino,[31] K. T. Pitts,[10] R. Plunkett,[10] A. Pompos,[33] L. Pondrom,[43] G. Pope,[32] F. Prokoshin,[8] J. Proudfoot,[2] F. Ptohos,[12] G. Punzi,[31] K. Ragan,[23] D. Reher,[21] A. Ribon,[29] F. Rimondi,[3] L. Ristori,[31] W. J. Robertson,[9] A. Robinson,[23] T. Rodrigo,[6] S. Rolli,[41] L. Rosenson,[22] R. Roser,[10] R. Rossin,[29] W. K. Sakumoto,[34] D. Saltzberg,[5] A. Sansoni,[12] L. Santi,[39] H. Sato,[40] P. Savard,[23] P. Schlabach,[10] E. E. Schmidt,[10] M. P. Schmidt,[44] M. Schmitt,[14] L. Scodellaro,[29] A. Scott,[5] A. Scribano,[31] S. Segler,[10] S. Seidel,[26] Y. Seiya,[40] A. Semenov,[8] F. Semeria,[3] T. Shah,[22] M. D. Shapiro,[21] P. F. Shepard,[32] T. Shibayama,[40] M. Shimojima,[40] M. Shochet,[7] J. Siegrist,[21] G. Signorelli,[31] A. Sill,[38] P. Sinervo,[23] P. Singh,[16] A. J. Slaughter,[44] K. Sliwa,[41] C. Smith,[17] F. D. Snider,[10] A. Solodsky,[35] J. Spalding,[10] T. Speer,[13] P. Sphicas,[22] F. Spinella,[31] M. Spiropulu,[14] L. Spiegel,[10] L. Stanco,[29] J. Steele,[43] A. Stefanini,[31] J. Strologas,[16] F. Strumia,[13] D. Stuart,[10] K. Sumorok,[22] T. Suzuki,[40] R. Takashima,[15] K. Takikawa,[40] M. Tanaka,[40] T. Takano,[28] B. Tannenbaum,[5] W. Taylor,[23] M. Tecchio,[24] P. K. Teng,[1] K. Terashi,[40] S. Tether,[22] D. Theriot,[10] R. Thurman-Keup,[2] P. Tipton,[34] S. Tkaczyk,[10] K. Tollefson,[34] A. Tollestrup,[10] H. Toyoda,[28] W. Trischuk,[23] J. F. de Troconiz,[14] S. Truitt,[24] J. Tseng,[22] N. Turini,[31] F. Ukegawa,[40] J. Valls,[36] S. Vejcik III,[10] G. Velev,[31] R. Vidal,[10] R. Vilar,[6] I. Vologouev,[21] D. Vucinic,[22] R. G. Wagner,[2] R. L. Wagner,[10] J. Wahl,[7] N. B. Wallace,[36] A. M. Walsh,[36] C. Wang,[9] C. H. Wang,[1] M. J. Wang,[1] T. Watanabe,[40] T. Watts,[36] R. Webb,[37] H. Wenzel,[18] W. C. Wester III,[10] A. B. Wicklund,[2] E. Wicklund,[10] H. H. Williams,[30] P. Wilson,[10] B. L. Winer,[27] D. Winn,[24] S. Wolbers,[10] D. Wolinski,[24] J. Wolinski,[25] S. Worm,[26] X. Wu,[13] J. Wyss,[31] A. Yagil,[10] W. Yao,[21] G. P. Yeh,[10] P. Yeh,[1] J. Yoh,[10] C. Yosef,[25] T. Yoshida,[28] I. Yu,[19] S. Yu,[30] A. Zanetti,[39] F. Zetti,[21] and S. Zucchelli[3]

(CDF Collaboration)

[1]*Institute of Physics, Academia Sinica, Taipei, Taiwan 11529, Republic of China*
[2]*Argonne National Laboratory, Argonne, Illinois 60439*
[3]*Istituto Nazionale di Fisica Nucleare, University of Bologna, I-40127 Bologna, Italy*
[4]*Brandeis University, Waltham, Massachusetts 02254*
[5]*University of California at Los Angeles, Los Angeles, California 90024*
[6]*Instituto de Fisica de Cantabria, University of Cantabria, 39005 Santander, Spain*
[7]*Enrico Fermi Institute, University of Chicago, Chicago, Illinois 60637*
[8]*Joint Institute for Nuclear Research, RU-141980 Dubna, Russia*
[9]*Duke University, Durham, North Carolina 27708*
[10]*Fermi National Accelerator Laboratory, Batavia, Illinois 60510*
[11]*University of Florida, Gainesville, Florida 32611*
[12]*Laboratori Nazionali di Frascati, Istituto Nazionale di Fisica Nucleare, I-00044 Frascati, Italy*
[13]*University of Geneva, CH-1211 Geneva 4, Switzerland*
[14]*Harvard University, Cambridge, Massachusetts 02138*
[15]*Hiroshima University, Higashi-Hiroshima 724, Japan*
[16]*University of Illinois, Urbana, Illinois 61801*
[17]*The Johns Hopkins University, Baltimore, Maryland 21218*
[18]*Institut für Experimentelle Kernphysik, Universität Karlsruhe, 76128 Karlsruhe, Germany*
[19]*Korean Hadron Collider Laboratory, Kyungpook National University, Taegu 702-701, Korea;*
Seoul National University, Seoul 151-742, Korea;
SungKyunKwan University, Suwon 440-746, Korea
[20]*High Energy Accelerator Research Organization (KEK), Tsukuba, Ibaraki 305, Japan*
[21]*Ernest Orlando Lawrence Berkeley National Laboratory, Berkeley, California 94720*
[22]*Massachusetts Institute of Technology, Cambridge, Massachusetts 02139*
[23]*Institute of Particle Physics, McGill University, Montreal, Canada H3A 2T8*
and University of Toronto, Toronto, Canada M5S 1A7
[24]*University of Michigan, Ann Arbor, Michigan 48109*
[25]*Michigan State University, East Lansing, Michigan 48824*
[26]*University of New Mexico, Albuquerque, New Mexico 87131*
[27]*The Ohio State University, Columbus, Ohio 43210*
[28]*Osaka City University, Osaka 588, Japan*
[29]*Universita di Padova, Istituto Nazionale di Fisica Nucleare, Sezione di Padova, I-35131 Padova, Italy*
[30]*University of Pennsylvania, Philadelphia, Pennsylvania 19104*
[31]*Istituto Nazionale di Fisica Nucleare, University and Scuola Normale Superiore of Pisa, I-56100 Pisa, Italy*
[32]*University of Pittsburgh, Pittsburgh, Pennsylvania 15260*
[33]*Purdue University, West Lafayette, Indiana 47907*
[34]*University of Rochester, Rochester, New York 14627*
[35]*Rockefeller University, New York, New York 10021*
[36]*Rutgers University, Piscataway, New Jersey 08855*
[37]*Texas A&M University, College Station, Texas 77843*
[38]*Texas Tech University, Lubbock, Texas 79409*
[39]*Istituto Nazionale di Fisica Nucleare, University of Trieste/Udine, Trieste, Italy*
[40]*University of Tsukuba, Tsukuba, Ibaraki 305, Japan*
[41]*Tufts University, Medford, Massachusetts 02155*
[42]*Waseda University, Tokyo 169, Japan*
[43]*University of Wisconsin, Madison, Wisconsin 53706*
[44]*Yale University, New Haven, Connecticut 06520*

The oscillation frequency Δm_d of $B^0 \bar{B}^0$ mixing is measured using the partially reconstructed semileptonic decay $\bar{B}^0 \rightarrow l^- \bar{\nu} D^{*+} X$. The data sample was collected with the CDF detector at the Fermilab Tevatron collider during 1992–1995 by triggering on the existence of two lepton candidates in an event, and corresponds to about 110 pb^{-1} of $\bar{p}p$ collisions at $\sqrt{s} = 1.8$ TeV. We estimate the proper decay time of the $\bar{B}^0$ meson from the measured decay length and reconstructed momentum of the $l^- D^{*+}$ system. The charge of the lepton in the final state identifies the flavor of the $\bar{B}^0$ meson at its decay. The second lepton in the event is used to infer the flavor of the $\bar{B}^0$ meson at production. We measure the oscillation frequency to be $\Delta m_d = 0.516 \pm 0.099^{+0.029}_{-0.035}$ ps^{-1}, where the first uncertainty is statistical and the second is systematic.
[S0556-2821(99)04623-8]

PACS number(s): 14.40.Nd, 13.20.He

I. INTRODUCTION

Particle-antiparticle mixing in the $B^0 \bar{B}^0$ system has been known for a decade now [1]. The phenomenon can be understood as a second-order weak interaction effect. The frequency of the oscillation between the two states corresponds to the mass difference Δm_d between the two mass eigenstates of the $B^0 \bar{B}^0$ system, B_H^0 and B_L^0. It can be calculated [2] from box diagrams, where contributions of the top quark in the loop are dominant. Measurements of $B^0 \bar{B}^0$ mixing can therefore determine the magnitude of the Kobayashi-Maskawa matrix [3] element V_{td}.

Experiments at the $\Upsilon(4S)$ resonance have measured the probability of mixing, χ_d, integrated over decay time [4]. Experiments at the CERN $e^+ e^-$ collider LEP [5,6] and the Collider Detector at Fermilab (CDF) [7], where B hadrons are produced at higher energies, examine the time development of mixing and measure the oscillation frequency Δm_d. By now the Δm_d measurements, as well as the top quark mass measurements, have become sufficiently precise that other uncertainties, in particular the B^0 meson decay constant, limit the precision of the extraction of $|V_{td}|$.

The same phenomenon of particle-antiparticle oscillations is expected for the $B_s^0 \bar{B}_s^0$ system, where the relevant element of the Kobayashi-Maskawa (KM) matrix is $|V_{ts}|$. Because of the difference in the involved matrix elements, $B_s^0 \bar{B}_s^0$ mixing is expected to proceed with a higher oscillation frequency, and so far only lower limits on the frequency Δm_s have been placed [6,8]. Once the $B_s^0 \bar{B}_s^0$ oscillation is established, a measurement of the ratio of the two oscillation frequencies, $\Delta m_s / \Delta m_d$, would provide a useful constraint on the ratio of the KM matrix elements $|V_{ts}|/|V_{td}|$ with less theoretical uncertainty.

In this paper we report a measurement of $B^0 \bar{B}^0$ mixing using partially reconstructed semileptonic decays. The data used in this analysis were collected in 1992–1995 with the CDF detector at the Fermilab Tevatron proton-antiproton collider at a center-of-mass energy of $\sqrt{s} = 1.8$ TeV, and correspond to an integrated luminosity of about 110 pb^{-1}. We use a data sample where events are selected requiring the existence of two lepton candidates. In order to identify semileptonic decays of $\bar{B}$ mesons, we select events with a lepton (e^- or μ^-, denoted by l^-) associated with a D^{*+} meson. (Throughout this paper a reference to a particular charge state also implies its charge conjugate.) The $l^- D^{*+}$ pairs consist mostly of $\bar{B}^0$ decays. The D^{*+} decays are reconstructed using the decay mode $D^{*+} \rightarrow D^0 \pi^+$, followed by $D^0 \rightarrow K^- \pi^+$, $K^- \pi^+ \pi^+ \pi^-$, or $K^- \pi^+ \pi^0$. About 500 such decays are reconstructed in the data sample. We reconstruct their decay vertices and estimate the proper decay length of the $\bar{B}^0$ meson using the momentum of the $l^- D^{*+}$ system. The charge of the final state lepton identifies the flavor of the $\bar{B}^0$ meson at the time of its decay ($l^- D^{*+}$ for $\bar{B}^0$, and $l^+ D^{*-}$ for B^0). The $\bar{B}^0$ meson flavor at its production is inferred from the charge of the second lepton in the event ($\bar{b} \rightarrow B \rightarrow l^+ \nu X$), assuming that b and $\bar{b}$ quarks are produced

in pairs. Thus, in ideal cases, an opposite-sign lepton pair identifies an unmixed decay, and a same-sign pair identifies a mixed decay. We examine decay length distributions of opposite-sign and same-sign events and extract the oscillation frequency Δm_d.

II. CDF DETECTOR AND TRIGGER

The CDF detector is described in detail elsewhere [9]. We describe here only the detector components most relevant to this analysis. Inside the 1.4 T solenoid the silicon vertex detector (SVX) [10] and the central tracking chamber (CTC) provide the tracking and momentum analysis of charged particles. The CTC is a cylindrical drift chamber containing 84 measurement layers. It covers the pseudorapidity interval $|\eta| < 1.1$, where $\eta = -\ln[\tan(\theta/2)]$. In CDF, φ is the azimuthal angle, θ is the polar angle measured from the proton direction, and r is the radius from the beam axis (z-axis). The SVX consists of four layers of silicon micro-strip detectors located at radii between 2.9 and 7.9 cm from the beam line and provides spatial measurements in the r-φ plane with a resolution of 13 μm. It gives a track impact parameter resolution of about $(13 + 40/p_T)$ μm [10], where p_T is the momentum of the track measured in the plane transverse to the beam axis and in units of GeV/c. The silicon detectors extend to ± 25 cm along the z axis, where z is parallel to the proton beam axis. Since the vertex distribution for $\bar{p}p$ collisions has an rms width of ± 30 cm along the z direction, a substantial fraction of the interactions occurs outside of the SVX coverage; as a result, the average geometric acceptance of the SVX is about 60%. The transverse profile of the Tevatron beam is circular and has an rms spread along both x and y axes of ~ 35 μm for the data taking period in 1992–1993 and ~ 25 μm in 1994–1995. The p_T resolution of the CTC combined with the SVX is $\sigma(p_T)/p_T = [(0.0066)^2 + (0.0009\, p_T)^2]^{1/2}$. Electromagnetic (CEM) and hadronic (CHA) calorimeters with projective tower geometry are located outside the solenoid and cover the pseudorapidity region $|\eta| < 1.1$, with a segmentation of $\Delta\varphi = 15°$ and $\Delta\eta \simeq 0.11$. A layer of proportional chambers (CES) is embedded near shower maximum in the CEM and provides a more precise measurement of electromagnetic shower profiles and an additional measurement of pulse height. A layer of proportional chambers (CPR) is also installed between the solenoid and the CEM and samples the electromagnetic showers at about one radiation length. Two muon subsystems in the central rapidity region ($|\eta| < 0.6$) are used for muon identification: the central muon chambers (CMU) located just behind the CHA calorimeter, and the central upgrade muon chambers (CMP) which lie behind an additional 60 cm of steel. The central muon extension chambers (CMX), covering a rapidity region up to $|\eta| < 1.0$, are also used.

CDF uses a three-level trigger system, where at the first two levels decisions are made with dedicated hardware. The information available at this stage includes energy deposits in the CEM and CHA calorimeters, high p_T tracks found in CTC by a track processor, and track segments found in the muon subsystems. At the third level of the trigger, the event selection is based on a version of off-line reconstruction pro-

grams optimized for speed. The lepton selection criteria used in level 3 are similar to those described in the next section.

Events containing semileptonic B decays and used for this analysis are collected using two triggers that require two lepton candidates in an event. The first trigger requires both an electron candidate and a muon candidate. The E_T threshold for the electron is 5 GeV, where $E_T \equiv E \sin \theta$, and E is the energy measured in the CEM. In addition, a track is required in the CTC with $p_T > 4.7$ GeV/c that points at the calorimeter tower in φ. The muon candidate requires a track in the CTC with matched track segments in the CMU or CMX system corresponding to a particle with $p_T > 2.7$ GeV/c. The second trigger requires two muon candidates, where the p_T threshold is 2.2 GeV/c for each muon, and at least one of the muons is required to have track segments in both the CMU and CMP chambers.

III. RECONSTRUCTION OF SEMILEPTONIC DECAYS OF B MESONS

The analysis starts with identification of lepton candidates. We require at least two good lepton candidates in an event. We then look for the charm meson D^{*+} associated with each lepton candidate to identify the $\bar{B}$ meson decay $\bar{B} \to l^- \bar{\nu} D^{*+} X$. A proper correlation between the lepton charge and the charm flavor; namely, l^- with D^{*+}, and not l^+ with D^{*+}, is required. This decay is used to measure the proper decay length of the $\bar{B}^0$ meson and to identify the decay flavor. The charge of the other lepton candidate in the event is used to infer the flavor of the $\bar{B}^0$ meson at its production.

A. Lepton identification

The identification of electrons makes use of information from both calorimeters and tracking chambers. We require the following:

Longitudinal shower profile consistent with electrons, i.e., small leakage of energy into the CHA.

Lateral shower profiles measured with the CEM [11] and the CES [12] consistent with test beam data.

Association of a high p_T track with the calorimeter shower based on position matching and energy-to-momentum ratio.

Pulse heights in the CES and CPR consistent with an electron. Photon conversion electrons, as well as the Dalitz decays of π^0 mesons, are removed by looking for oppositely charged tracks that have small opening angles with the electron candidate.

Muons are identified based on the geometrical match between the track segments in the muon chambers and an extrapolated CTC track. We compute the χ^2 of the matching, where the number of degrees of freedom is one and the uncertainty is dominated by multiple Coulomb scattering in the detector material. We require $\chi^2 < 9$ in the r-φ view (CMU and CMP) and $\chi^2 < 12$ in the r-z view (CMU). For muon candidates in the CMX we require $\chi^2 < 9$ in both the r-φ and r-z views.

B. Charm meson reconstruction

To identify $\bar{B} \to l^- \bar{\nu} D^{*+} X$ candidates, we search for $D^{*+} \to D^0 \pi^+$ decays in the vicinity of a lepton candidate using two fully reconstructed D^0 decay modes, $D^0 \to K^- \pi^+$ and $D^0 \to K^- \pi^+ \pi^+ \pi^-$, and one partially reconstructed mode, $D^0 \to K^- \pi^+ \pi^0$. To reconstruct $D^0 \to K^- \pi^+$ decays, we first select oppositely charged pairs of particles using CTC tracks, where the kaon mass is assigned to the particle with the same charge as the lepton, as is the case in semileptonic B decays. The kaon (pion) candidate is then required to have transverse momentum above 1.2 (0.4) GeV/c, and to be within a cone of radius $\Delta R = 0.8$ (1.0) around the lepton in η-φ space, where $\Delta R = [(\Delta \eta)^2 + (\Delta \varphi)^2]^{1/2}$. To ensure accurate decay length measurement, each candidate track, as well as the lepton track, is required to be reconstructed in the SVX with hits in at least two layers out of the possible four, and with $\chi^2 < 6$ per hit where the number of degrees of freedom is one. To reduce combinatorial background, we require the decay vertex of the D^0 candidate to be positively displaced along its flight direction in the transverse plane with respect to the position of the primary vertex. The primary vertex is approximated by the position of the Tevatron beam, which has been determined using independent events [14]. For the $D^0 \to K^- \pi^+ \pi^+ \pi^-$ mode, the kaon (pion) candidate is required to have transverse momentum above 1.2 (0.5) GeV/c, and to be within a cone of radius $\Delta R = 0.6$ (1.0) around the lepton candidate. For the $D^0 \to K^- \pi^+ \pi^0$ mode, the kaon (pion) candidate is required to have transverse momentum above 1.2 (0.4) GeV/c, and to be within a cone of radius $\Delta R = 0.7$ (0.8) around the lepton candidate.

In order to qualify as a candidate for the signal, the D^0 candidate has to be in the mass range 1.83 to 1.90 GeV/c^2 for the fully reconstructed mode $D^0 \to K^- \pi^+$ and in the range 1.84 to 1.88 GeV/c^2 for the $\to K^- \pi^+ \pi^+ \pi^-$ mode. For the partially reconstructed mode $D^0 \to K^- \pi^+ \pi^0$, we require the mass of a $K^- \pi^+$ pair to be between 1.5 and 1.7 GeV/c^2; we do not reconstruct the π^0 meson and in the subsequent analysis treat the $K^- \pi^+$ pair as if it were a D^0 meson. For each mode, we reconstruct the D^{*+} meson by combining an additional CTC track, assumed to have the pion mass, with the D^0 candidate, and computing the mass difference, ΔM, between the $D^0 \pi^+$ and D^0 candidates. Figure 1 shows the ΔM distributions for the three D^0 decay modes. In Fig. 1(c) the peak is broadened because of the missing π^0 meson. The dotted histograms show the spectra from the ''wrong sign'' ($D^0 \pi^-$) combinations, where no significant signals are observed. We define the signal region as follows: the two fully reconstructed modes use the ΔM range 0.144–0.147 GeV/c^2, and the $K^- \pi^+ \pi^0$ mode uses the range $\Delta M < 0.155$ GeV/c^2. The numbers of events in the signal regions are 216, 256, and 416 for the three modes. We estimate the numbers of combinatorial background events by using the shapes of the ΔM spectra of the wrong sign ($D^0 \pi^-$) combinations and normalizing them to the number of events in the ΔM sideband. The estimated background fractions are 0.227 ± 0.036, 0.326 ± 0.040, and 0.543 ± 0.050, respectively. They are summarized in Table I.
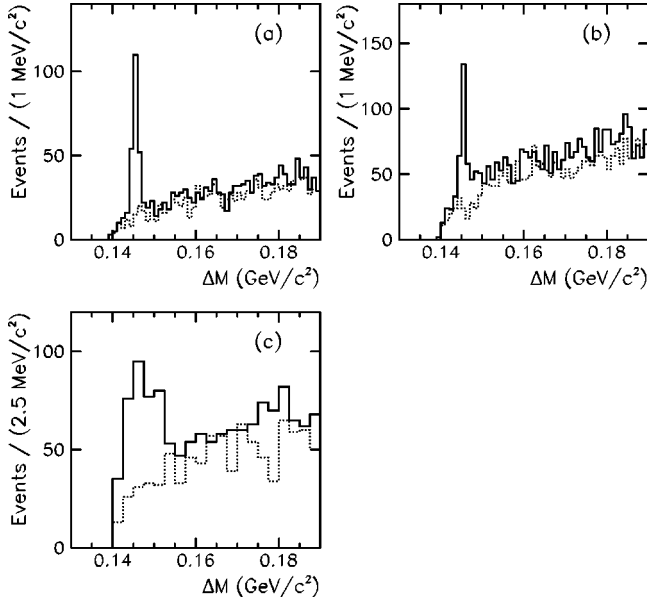
FIG. 1. Reconstructed $D^{*+}\rightarrow D^0\pi^+$ signals in events with two lepton candidates. The D^{*+} meson is associated with a lepton (l^-) candidate. Distributions of ΔM for three D^0 decay modes are shown: (a) $D^0\rightarrow K^-\pi^+$, (b) $D^0\rightarrow K^-\pi^+\pi^+\pi^-$, and (c) $D^0\rightarrow K^-\pi^+\pi^0$. Dotted histograms show the distributions for wrong sign ($D^0\pi^-$) combinations.

C. Sample composition

Apart from combinatorial backgrounds, the l^-D^{*+} signal sample contains events which originated from physics sources other than the $\bar{B}^0$ meson decays. The main contribution comes from B^- meson decays. The semileptonic decays of B mesons can be expressed as $\bar{B}\rightarrow l^-\bar{\nu}\mathbf{D}$, where $\mathbf{D}$ is a charm system whose charge is correlated with the B meson charge. If only the two lowest mass charm states, pseudoscalar (D) and vector (D^*) mesons, are produced, the l^-D^{*+} combination can arise only from the $\bar{B}^0$ decay. However, it has been known that the above two lowest mass states do not saturate the total semileptonic decay rates. All data indicate that higher mass charm mesons, D^{**} states, as well as non-resonant $D^{(*)}\pi$ pairs, are responsible for the rest of the semileptonic decays [13]. In this analysis we do not distinguish resonant and non-resonant components, and refer to both of them as D^{**} mesons.

These D^{**} meson decays can dilute the charge correlation between the final states and the parent B meson. For example, the D^{**0} meson can be produced by the decay $B^-\rightarrow l^-\bar{\nu}D^{**0}$, which subsequently can produce both $D^{*+}\pi^-$ and $D^{*0}\pi^0$ final states. This results in misidentification of the B^- meson decay as $\bar{B}^0\rightarrow D^{*+}l^-\bar{\nu}X$. Nevertheless, the l^-D^{*+} combination is dominated by $\bar{B}^0$ meson decays.

In order to estimate the fraction g^- of B^- decays relative to the sum of B^- and $\bar{B}^0$ mesons in the observed l^-D^{*+} sample, we follow the method used in the CDF measurement of the B^- and $\bar{B}^0$ meson lifetimes [15] using semileptonic decays. We describe the method here as well.

The production rates of charged and neutral B mesons and their semileptonic decay widths are assumed to be equal. We also assume the D^{**} mesons decay exclusively to a $D^{(*)}\pi$ pair via the strong interaction, thereby allowing us to determine the branching fractions, e.g., $D^{(*)+}\pi^0$ vs $D^{(*)0}\pi^+$, using isospin symmetry. We consider three factors affecting the composition. First, the composition depends on the fraction f^{**} of the D^{**} mesons produced in semileptonic B decays,

$$f^{**}\equiv\frac{\mathcal{B}(\bar{B}\rightarrow l^-\bar{\nu}D^{**})}{\mathcal{B}(\bar{B}\rightarrow l^-\bar{\nu}DX)}$$

$$=1-\frac{\mathcal{B}(\bar{B}\rightarrow l^-\bar{\nu}D)+\mathcal{B}(\bar{B}\rightarrow l^-\bar{\nu}D^*)}{\mathcal{B}(\bar{B}\rightarrow l^-\bar{\nu}DX)},$$

where $\mathcal{B}$ denotes a branching fraction and $\bar{B}$ is a B^- or $\bar{B}^0$ meson. The CLEO experiment measures the fraction of exclusive decays to the two lowest mass states to be $0.64\pm0.10\pm0.06$ [16]. Thus, we estimate that $f^{**}=0.36\pm0.12$. A few experiments have recently observed some D^{**} modes [17], but the sum of exclusive modes still does not equal the total semileptonic rate. Second, the fraction g^- depends on the relative abundance of various possible D^{**} states, because some of them decay only to $D^*\pi$ and others to $D\pi$, depending on the spin and parity. The abundance is not measured very well at present. Changing the abundance is equivalent to changing the branching fractions for $D^*\pi$ and $D\pi$ modes averaged over various D^{**} states. We define the quantity

$$P_V\equiv\frac{\mathcal{B}(D^{**}\rightarrow D^*\pi)}{\mathcal{B}(D^{**}\rightarrow D^*\pi)+\mathcal{B}(D^{**}\rightarrow D\pi)}.$$

We assume the relative abundance of the four D^{**} mesons predicted by the Isgur-Scora-Grinstein-Wise (ISGW) model [18], which corresponds to $P_V=0.64$. After inclusion of non-resonant contributions, we use $P_V=0.65$ as our nominal

TABLE I. Definition of signal samples, numbers of candidates and estimated background fractions.

B mode	D^0 mode	D^0 mass range (GeV/c^2)	ΔM range (GeV/c^2)	Events	Background fraction
l^-D^{*+}	$K^-\pi^+$	$1.83-1.90$	$0.144-0.147$	216	0.227 ± 0.036
l^-D^{*+}	$K^-\pi^+\pi^+\pi^-$	$1.84-1.88$	$0.144-0.147$	256	0.326 ± 0.040
l^-D^{*+}	$K^-\pi^+\pi^0$	$1.50-1.70$	<0.155	416	0.543 ± 0.050

choice. We also consider the values $P_V = 0.26$ and 1.00. Third, the composition depends on the ratio of the B^- and $\bar{B}^0$ meson lifetimes, because the number of $l^- D^{*+}$ events is proportional to the semileptonic branching fraction, which is the product of the lifetime and the partial width. We use the ratio $\tau(B^-)/\tau(\bar{B}^0) = 1.02 \pm 0.05$ [19].

We also take into account the differences in the reconstruction efficiencies for the $\bar{B} \to l^- \bar{\nu} D^*$ and D^{**} decay modes. We examine this effect by using Monte Carlo events where the ISGW model is used to describe the semileptonic decays. We shall describe the Monte Carlo simulation later. We find that the efficiency for the D^{**} mode is lower than that for the D^* mode by about 50% (25%) for leptons above 5 GeV/c (2 GeV/c).

We find that $g^- = 0.19^{+0.08}_{-0.10}$ for the $\mu^- D^{*+}$ sample and $g^- = 0.14^{+0.06}_{-0.08}$ for the $e^- D^{*+}$ sample. The central values correspond to the nominal choice of the parameters, $f^{**} = 0.36$, $P_V = 0.65$, and $\tau(B^-)/\tau(\bar{B}^0) = 1.02$. The uncertainties reflect maximum changes in g^- when f^{**}, P_V and the lifetime ratio are changed within their uncertainties, namely f^{**} to 0.24 and 0.48, P_V to 0.26 and 1.0, and $\tau(B^-)/\tau(\bar{B}^0)$ to 0.97 and 1.07. The difference between the muon and electron channels arises from the difference in kinematic requirements.

There are other physics processes that can produce the lepton-D^{*+} signature. The largest background comes from the decay of the $\bar{B}_s^0$ meson, $\bar{B}_s^0 \to l^- \bar{\nu} D_s^{**+}$, followed by $D_s^{**+} \to D^{*+} K^0$. This process is estimated to contribute about 3% of the lepton-D^{*+} signal. Other processes such as $\bar{B} \to \tau^- \bar{\nu}_\tau D^{*+} X$ followed by $\tau^- \to l^- \bar{\nu}_l \nu_\tau$, and $\bar{B} \to D_s^- D^{*+} X$ followed by $D_s^- \to l^- X$, are suppressed severely because of branching fractions and kinematic requirements on leptons. We ignore these backgrounds here. Therefore, the fraction of $\bar{B}^0$ mesons is given by $g^0 = 1 - g^-$. We treat effects of the physics backgrounds as a systematic uncertainty.

IV. DECAY LENGTH MEASUREMENT AND MOMENTUM ESTIMATE

The B meson decay vertex $\vec{V}_B$ is obtained by intersecting the trajectory of the lepton track with the flight path of the D^0 candidate. The pion from the D^{*+} decay is not used in the vertex determination because it is almost parallel to the D^0 meson, due to the small Q value of the decay, and thus provides little improvement in the vertex resolution. The B decay length L_B is defined as the displacement of $\vec{V}_B$ from the primary vertex $\vec{V}_P$, measured in the plane perpendicular to the beam axis, and projected onto the transverse momentum vector of the lepton-D^{*+} system:

$$L_B \equiv \frac{(\vec{V}_B - \vec{V}_P) \cdot \vec{p}_T^{\, l^- D^{*+}}}{p_T^{\, l^- D^{*+}}}.$$

A schematic representation of the $\bar{B}^0$ meson semileptonic decay is illustrated in Fig. 2.

To measure the proper decay length of a B meson, we need to know the momentum of the B meson. In semileptonic decays, the B meson momentum cannot be measured precisely because of the missing neutrino. We use the transverse momentum of the observed system, $p_T^{\, l^- D^{*+}}$, to estimate the B meson transverse momentum p_T^B for each event. We denote the ratio of the two momenta by $K \equiv p_T^{\, l^- D^{*+}}/p_T^B$, and introduce a corrected decay length defined as

$$x \equiv L_B \frac{m_B}{p_T^{\, l^- D^{*+}}} \langle K \rangle,$$

which we call the ''pseudo-proper decay length.'' The average correction for the missing momentum is achieved by the constant $\langle K \rangle$. The correction for a finite width of the distribution of the ratio K is performed during fits to decay length distributions. We shall describe the fits later.

A typical resolution on this decay length x due to vertex determination is 50 μm, including the contribution from the finite size of the primary vertex. For subsequent decay length measurements, we use only those events in which the resolutions on reconstructed decay lengths are smaller than 0.05 cm. We also require the proper decay length of the D^0 meson, measured from the B meson decay vertex to the D^0 decay vertex, to be in the range from -0.1 cm to 0.1 cm, with its uncertainty smaller than 0.05 cm. These cuts reject poorly measured decays and reduce random track combinations. In addition, we limit ourselves to events with reconstructed decay lengths in the range between -0.15 cm and 0.3 cm. These cuts have been applied already for the charm signals shown in Fig. 1.

The distribution of the momentum ratio K is obtained from a Monte Carlo simulation. The b quarks are generated according to the p_T spectrum by the QCD calculation in the next-to-leading order [20]. The fragmentation model by Peterson and others [21] is used. The CLEO event generator [22] is then used to describe the B meson decays. In particular, the semileptonic decays adopt the ISGW model [18]. The K distributions obtained for the $\bar{B}^0$ meson decays are shown in Fig. 3. A typical K distribution has an average value of 0.85 with an rms width of 0.14, and shows only a weak dependence on $p_T^{\, l^- D^{*+}}$ in the range of interest, which is typically between 10 and 20 GeV/c^2. It is also independent of the D^0 decay mode except for the partially reconstructed mode $D^0 \to K^- \pi^+ \pi^0$, which has a slightly lower mean value (about 0.80) because of the missing π^0 meson. The K distributions for the B^- decays are similar, but have slightly lower mean values because of additional missing particle(s).

We fit the observed pseudo-proper decay length distributions for both opposite-sign and same-sign events. This fit determines parameters that will be used later in the fit for the oscillation frequency Δm_d. It also yields the B^0 meson lifetime as a check of the momentum correction described above. We use the maximum likelihood method. The likelihood used to fit the events in the signal region is expressed as
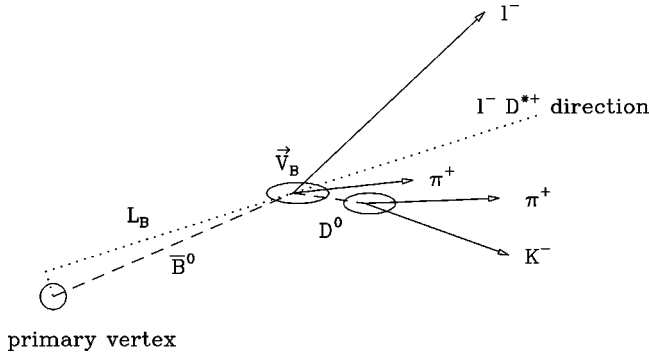
FIG. 2. Schematic representation of the decay $\bar{B}^0 \rightarrow l^- \bar{\nu} D^{*+}$, followed by $D^{*+} \rightarrow D^0 \pi^+$ and $D^0 \rightarrow K^- \pi^+$.

$$\mathcal{L}_{\text{SIG}} = \prod_i \ [(1-f_{\text{BG}})\mathcal{F}_{\text{SIG}}(x_i) + f_{\text{BG}}\mathcal{F}_{\text{BG}}(x_i)],$$

where x_i is the pseudo-proper decay length measured for event i, and the product is taken over observed events in the sample. The first term in the likelihood function represents the contribution of B decay signal events, while the second term accounts for combinatorial background events whose fraction in the sample is f_{BG}.

The signal probability density function $\mathcal{F}_{\text{SIG}}(x)$ has two components and is expressed as

$$\mathcal{F}_{\text{SIG}}(x) = g^- \mathcal{F}_{\text{SIG}}^-(x) + (1-g^-)\mathcal{F}_{\text{SIG}}^0(x),$$

where $\mathcal{F}_{\text{SIG}}^-(x)$ and $\mathcal{F}_{\text{SIG}}^0(x)$ are the normalized probability density functions for the B^- and $\bar{B}^0$ meson decays, respectively, and g^- is the fraction of B^- mesons as defined earlier. Each component consists of an exponential decay function, defined for positive decay lengths, smeared with a normalized K distribution $D(K)$ and a Gaussian distribution with width $s\sigma_i$:

$$\mathcal{F}_{\text{SIG}}^{-,0}(x) = \int dK \, D^{-,0}(K) \left[\theta(x) \frac{K}{c\tau\langle K \rangle} \right.$$
$$\left. \times \exp\left(-\frac{Kx}{c\tau\langle K \rangle} \right) \otimes G(x) \right], \qquad (1)$$

where τ is the appropriate B meson lifetime, c is the speed of light, $\theta(x)$ is the step function defined as $\theta(x)=1$ for $x \geq 0$ and $\theta(x)=0$ for $x<0$, and the symbol "$\otimes$" denotes a convolution. $G(x)$ is the Gaussian distribution given by

$$G(x) = \frac{1}{s\sigma_i\sqrt{2\pi}} \exp\left(-\frac{x^2}{2s^2\sigma_i^2} \right),$$

where σ_i is the estimated resolution on x_i. The scale factor s is introduced in order to account for a possible incompleteness of our estimate of the decay length resolution. The integration over the momentum ratio K is approximated by a finite sum
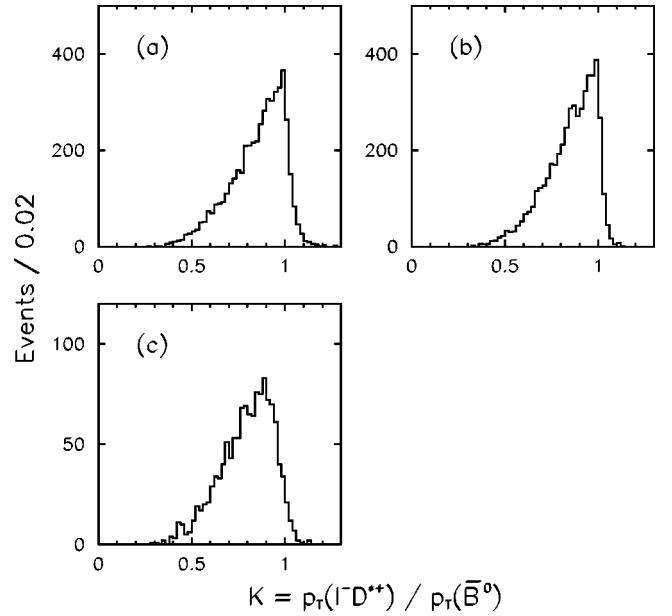

FIG. 3. Distributions of the momentum ratio K (see text) obtained from Monte Carlo simulations for decays $\bar{B}^0 \rightarrow l^- \bar{\nu} D^{*+} X$, followed by $D^{*+} \rightarrow D^0 \pi^+$. Three D^0 decay modes are shown: (a) $D^0 \rightarrow K^- \pi^+$, (b) $D^0 \rightarrow K^- \pi^+ \pi^+ \pi^-$, and (c) $D^0 \rightarrow K^- \pi^+ \pi^0$.

$$\int dK D(K) \rightarrow \sum_j \ D(K_j)\Delta K,$$

where the sum is taken over bin j of a histogrammed distribution $D(K_j)$ with bin width $\Delta K = 0.02$. The K distributions for B^- and $\bar{B}^0$ mesons are slightly different because the $B^- \rightarrow l^- \bar{\nu} D^{*+} X$ decay involves more missing particles.

The pseudo-proper decay length distribution of combinatorial background events, $\mathcal{F}_{\text{BG}}(x)$, is measured using ΔM sideband events, assuming that they represent the combinatorial background events under the signal mass peaks. The functional form of the distribution is parametrized empirically by a sum of a Gaussian distribution centered at zero, and positive and negative exponential tails smeared with a Gaussian distribution:

$$\mathcal{F}_{\text{BG}}(x) = (1 - f_- - f_+) \, G(x) + \frac{f_+}{\lambda_+} \theta(x)\exp\left(-\frac{x}{\lambda_+} \right)$$
$$\otimes G(x) + \frac{f_-}{\lambda_-} \theta(-x)\exp\left(+\frac{x}{\lambda_-} \right) \otimes G(x). \quad (2)$$

The shape of the background function (parameters $f_{\pm}$ and $\lambda_{\pm}$) and the resolution scale factor s, as well as the B meson lifetime $c\tau$, are determined from a simultaneous fit to signal and sideband events. We fix the ratio of the B^- and $\bar{B}^0$ meson lifetimes and fit for the $\bar{B}^0$ meson lifetime only. To determine those parameters, we use the combined likelihood $\mathcal{L}$ defined as $\mathcal{L} = \mathcal{L}_{\text{SIG}} \mathcal{L}_{\text{BG}}$, where $\mathcal{L}_{\text{BG}} = \Pi_k \mathcal{F}_{\text{BG}}(x_k)$ and the product is taken over event k in the background sample. The amount of combinatorial background f_{BG} is also a parameter in the simultaneous fit. This parameter is constrained by add-

TABLE II. Definition of background samples and numbers of events.

B mode	D^0 mode	D^0 mass range (GeV/c^2)	ΔM range (GeV/c^2) $D^0\pi^+$	ΔM range (GeV/c^2) $D^0\pi^-$	Events
l^-D^{*+}	$K^-\pi^+$	$1.83-1.90$	$0.15-0.19$	<0.19	2418
l^-D^{*+}	$K^-\pi^+\pi^+\pi^-$	$1.84-1.88$	$0.15-0.19$	<0.19	5139
l^-D^{*+}	$K^-\pi^+\pi^0$	$1.50-1.70$	$0.16-0.19$	<0.19	1663

ing a term $\frac{1}{2}\chi^2=\frac{1}{2}(f_{\mathrm{BG}}-\langle f_{\mathrm{BG}}\rangle)^2/\sigma^2_{\mathrm{BG}}$ to the negative log-likelihood $-l=-\ln\mathcal{L}$. The average background fraction $\langle f_{\mathrm{BG}}\rangle$ and its uncertainty σ_{BG} are estimated from the signal mass distributions and are given in Table I.

The background sample for the l^-D^{*+} candidates is taken from the ΔM sidebands: we use the right sign ($D^0\pi^+$) sideband $0.15<\Delta M<0.19$ GeV/c^2 for the two fully reconstructed D^0 modes, and $0.16<\Delta M<0.19$ GeV/c^2 for the $D^0\to K^-\pi^+\pi^0$ mode. We also use the wrong sign pion combinations in the range $\Delta M<0.19$ GeV/c^2 for all three D^0 decay modes. The background samples are summarized in Table II.

The pseudo-proper decay length distributions of the background samples are shown in Fig. 4, together with fit results. The background parameter values and the resolution scale s determined from the fit are listed in Table III. The corresponding decay length distributions of the signal samples are shown in Fig. 5. We find the lifetimes to be $c\tau(\bar{B}^0)=470\pm44$, 407 ± 40 and 419 ± 39 μm for the three D^0 decay modes. The quoted uncertainties are statistical only. When a combined fit to the three modes is made, we find $c\tau(\bar{B}^0)=433\pm24$ μm. These results are consistent with the world average value of 468 ± 12 μm [13].

V. $B^0\bar{B}^0$ MIXING MEASUREMENT

The probability that a $\bar{B}^0$ meson at $t=0$ decays as $\bar{B}^0$ (unmixed) or as B^0 (mixed) at a proper time t is given by

$$P_{\mathrm{UNM}}(t)=\frac{1}{2\tau}\exp\left(-\frac{t}{\tau}\right)(1+\cos\Delta m_d t),$$

$$P_{\mathrm{MIX}}(t)=\frac{1}{2\tau}\exp\left(-\frac{t}{\tau}\right)(1-\cos\Delta m_d t),$$

where τ is the $\bar{B}^0$ meson lifetime, and we have ignored CP violation and the width difference $\Delta\Gamma$ between the two mass eigenstates of the $B^0\bar{B}^0$ system. We determine the mixing parameter Δm_d by a simultaneous fit to the decay length distributions of unmixed and mixed decay events.

We have reconstructed the $\bar{B}^0$ meson decay $\bar{B}^0\to l^-\bar{\nu}D^{*+}X$. The charge of the lepton identifies the flavor of the B^0 meson at its decay. In order to infer the $\bar{B}^0$ meson flavor at its production, we use the second lepton candidate, which is presumed to originate from the other B hadron in the event. When the other B hadron, containing the $\bar{b}$ quark, decays semileptonically, it produces a positively charged

lepton l^+. If the $\bar{B}^0$ meson, reconstructed in the $l^-\bar{\nu}D^{*+}X$ decay mode, decayed in an unmixed state, the two leptons in the event would have the opposite charge. Similarly, if the $\bar{B}^0$ meson decayed in a mixed state, the leptons would have the same charge. Therefore, in the ideal case, the opposite-sign (OS) events identify the unmixed decays of the $\bar{B}^0$ meson, while the same-sign (SS) events identify the mixed decays. However, the second lepton can originate from the sequential decay of B hadrons, $\bar{b}\to\bar{c}\to l^-X$, or from a mixed decay of the neutral B mesons, $\bar{b}\to B^0(B^0_s)\to\bar{B}^0(\bar{B}^0_s)\to l^-X$. The lepton candidate could also be a misidentified hadron. In these cases the second lepton candidate will not identify the production flavor correctly. In order to account for these possibilities, we introduce the probability of flavor misidentification and denote it by W.

As mentioned above, we classify events depending on the sign (OS or SS) of the two lepton candidates in an event. A finite flavor misidentification probability W results in moving unmixed decay to the same-sign sample and mixed decays to the opposite-sign sample. Thus, we obtain the following
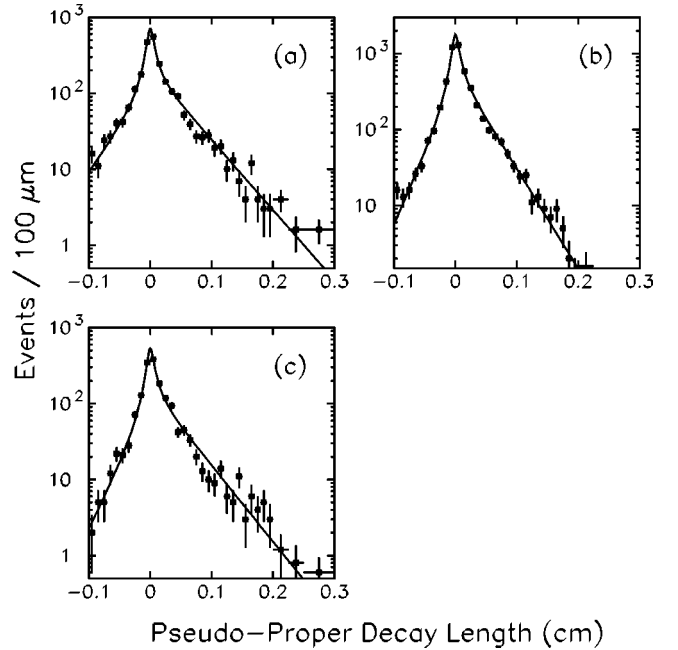

FIG. 4. Distributions of B meson pseudo-proper decay lengths for l^-D^{*+} background samples (points). Three decay modes are shown: (a) $D^{*+}\to D^0\pi^+$, $D^0\to K^-\pi^+$, (b) $D^{*+}\to D^0\pi^+$, $D^0\to K^-\pi^+\pi^+\pi^-$, and (c) $D^{*+}\to D^0\pi^+$, $D^0\to K^-\pi^+\pi^0$. Curves show fit results.

TABLE III. Background shapes obtained from a simultaneous fit to signal and background samples.

B mode	D^0 mode	scale s	f_+	λ_+ (μm)	f_-	λ_- (μm)
$l^- D^{*+}$	$K^- \pi^+$	1.21 ± 0.05	0.361 ± 0.015	474 ± 20	0.157 ± 0.015	392 ± 49
$l^- D^{*+}$	$K^- \pi^+ \pi^+ \pi^-$	1.17 ± 0.03	0.332 ± 0.012	331 ± 11	0.098 ± 0.010	230 ± 22
$l^- D^{*+}$	$K^- \pi^+ \pi^0$	1.21 ± 0.04	0.367 ± 0.016	433 ± 22	0.095 ± 0.014	293 ± 33

probability distributions for the opposite-sign and same-sign events:

$$P^{\mathrm{OS}}(t) = (1-W)P_{\mathrm{UNM}}(t) + WP_{\mathrm{MIX}}(t)$$

$$= \frac{1}{2\tau} \exp\left(-\frac{t}{\tau}\right)[1 + (1-2W)\cos\Delta m_d t],$$

$$P^{\mathrm{SS}}(t) = (1-W)P_{\mathrm{MIX}}(t) + WP_{\mathrm{UNX}}(t)$$

$$= \frac{1}{2\tau} \exp\left(-\frac{t}{\tau}\right)[1 - (1-2W)\cos\Delta m_d t].$$

From these expressions it is evident that the flavor misidentification probability does not affect the oscillation frequency, although it does reduce its amplitude by a factor $1-2W$. We determine the two quantities that appear in the above expression, Δm_d and W, simultaneously from the data sample by examining the decay length distributions.
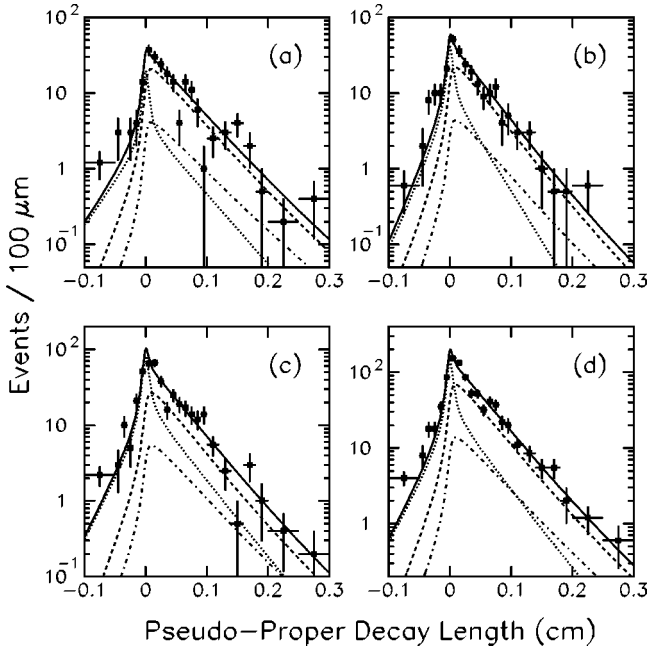

FIG. 5. Distributions of B meson pseudo-proper decay lengths for $l^- D^{*+}$ signal samples (points). Three decay modes are shown: (a) $D^{*+} \rightarrow D^0 \pi^+$, $D^0 \rightarrow K^- \pi^+$, (b) $D^{*+} \rightarrow D^0 \pi^+$, $D^0 \rightarrow K^- \pi^+ \pi^+ \pi^-$, and (c) $D^{*+} \rightarrow D^0 \pi^+$, $D^0 \rightarrow K^- \pi^+ \pi^0$. The three modes are combined in (d). Also shown are the results of lifetime fits: the $\bar{B}^0$ component (dashed curve), the B^- component (dot-dashed curve), the background component (dotted curve), and the sum of all components (solid curve).

A. Δm_d fit

We use the maximum likelihood method to extract the oscillation frequency Δm_d. The likelihood is given by $\mathcal{L} = \Pi_i \mathcal{F}(x_i)$, where x_i is the pseudo-proper decay length measured for event i, and the product is taken over events in the signal sample. The likelihood function $\mathcal{F}(x)$ is expressed as follows, depending on the sign (OS or SS) of an event:

$$\mathcal{F}(x) = \begin{cases} (1-f_{\mathrm{BG}})\mathcal{F}^{\mathrm{OS}}_{\mathrm{SIG}}(x) + f_{\mathrm{BG}}(1-f_{\mathrm{SS}})\mathcal{F}_{\mathrm{BG}}(x) & \text{if OS,} \\ (1-f_{\mathrm{BG}})\mathcal{F}^{\mathrm{SS}}_{\mathrm{SIG}}(x) + f_{\mathrm{BG}}f_{\mathrm{SS}}\mathcal{F}_{\mathrm{BG}}(x) & \text{if SS,} \end{cases}$$

where f_{BG} is the fraction of combinatorial background events in the sample. The background function $\mathcal{F}_{\mathrm{BG}}(x)$ is the same as in the lifetime fit [Eq. (2)], and its shape is taken to be the same for both opposite-sign and same-sign events. f_{SS} is the fraction of same-sign events in the combinatorial background.

Each of the signal functions consists of two components, one for the $\bar{B}^0$ meson and the other for the B^- meson:
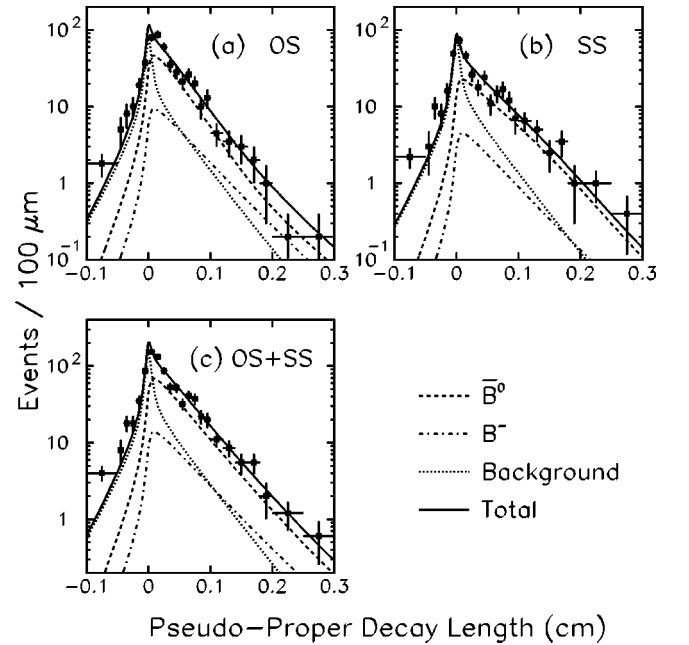

FIG. 6. B meson pseudo-proper decay length distribution (points) estimated from the $l^- D^{*+}$ candidates for (a) opposite-sign events, and (b) same-sign events, and (c) the sum of the two. Curves show the result of the Δm_d fit: the $\bar{B}^0$ component (dashed curve), the B^- component (dot-dashed curve), the background component (dotted curve), and the sum of all components (solid curve).

TABLE IV. Numbers of opposite-sign (OS) and same-sign (SS) events in the signal and background samples, and the fraction f_{SS} of same-sign events in the combinatorial background.

B mode	D^0 mode	Signal			Background		
		Sum	OS	SS	OS	SS	f_{SS}
$l^- D^{*+}$	$K^- \pi^+$	216	121	95	1240	1178	0.487 ± 0.010
$l^- D^{*+}$	$K^- \pi^+ \pi^+ \pi^-$	256	146	110	2501	2638	0.513 ± 0.007
$l^- D^{*+}$	$K^- \pi^+ \pi^0$	416	231	185	902	761	0.458 ± 0.012
$l^- D^{*+}$	Total	888	498	390			

$$\mathcal{F}_{SIG}^{OS}(x) = (1 - g^-) \left[(1 - W) \mathcal{F}_{UNM}^0(x) + W \mathcal{F}_{MIX}^0(x) \right]$$
$$+ g^- (1 - W) \mathcal{F}^-(x),$$

$$\mathcal{F}_{SIG}^{SS}(x) = (1 - g^-) \left[(1 - W) \mathcal{F}_{MIX}^0(x) + W \mathcal{F}_{UNM}^0(x) \right]$$
$$+ g^- W \mathcal{F}^-(x),$$

where g^- is the fraction of B^- meson decays among the signal, and W is the flavor misidentification probability of the second lepton. The $\bar{B}^0$ component of the opposite-sign function $\mathcal{F}_{SIG}^{OS}(x)$ contains two terms: the first term represents correctly tagged unmixed decays (probability $1 - W$), while the second term represents incorrectly tagged mixed decays (probability W). Similarly, the $\bar{B}^0$ component of the same-sign function $\mathcal{F}_{SIG}^{SS}(x)$ consists of correctly tagged mixed decays and incorrectly tagged unmixed decays. Since the B^- meson does not mix, it appears in the opposite-sign function when the production flavor is tagged correctly, and in the same-sign function when tagged incorrectly. The B^- function $\mathcal{F}^-(x)$ is a smeared exponential decay function and is the same as in the lifetime fit [Eq. (1)]. The $\bar{B}^0$ functions have an additional factor for the mixing and are given by

$$\mathcal{F}_{UNM,MIX}^0(x) = \int dK \, D(K) \left\{ \theta(x) \frac{K}{2c\tau\langle K \rangle} \exp\left(-\frac{Kx}{c\tau\langle K \rangle} \right) \right.$$
$$\left. \times \left[1 \pm \cos\left(\frac{\Delta m_d}{c} \frac{K}{\langle K \rangle} x \right) \right] \otimes G(x) \right\},$$

where the sign $+$ $(-)$ before the cosine corresponds to the unmixed (mixed) decay function. The background and B^- functions are normalized so as to give unity when integrated

over x. The B^0 functions give unity when integrated over x and summed over the two decay possibilities, unmixed and mixed. The free parameters in the fit are the oscillation frequency Δm_d and the flavor misidentification probability W. We fix the shape of the background function (parameters $f_\pm$ and $\lambda_\pm$) and the resolution scale factor as determined from the background sample. The lifetime of the B^0 meson is also fixed to the value determined earlier in the signal sample. This procedure has been found [23] to improve slightly the sensitivity in Δm_d determination. It is confirmed with our study using Monte Carlo events. The background fraction f_{BG} in the sample and the same-sign fraction f_{SS} of the background are fit parameters, but they are constrained by adding a χ^2 term to the negative log-likelihood $-l = -\ln\mathcal{L}$, as in the lifetime fits.

The B meson pseudo-proper decay length distributions of the $l^- D^{*+}$ signal sample are shown in Fig. 6 for the opposite-sign and same-sign events, as well as for the sum of the two. The three D^0 decay modes are combined there. We find 498 opposite-sign events and 390 same-sign events. The fraction of same-sign events in the combinatorial background, f_{SS}, is estimated using events in the background sample. The estimated same-sign fractions f_{SS} are summarized in Table IV. The fit results are $\Delta m_d = 0.516 \pm 0.099$ ps^{-1} and $W = 0.325 \pm 0.033$, where uncertainties are statisti-

TABLE V. Results of the Δm_d fit.

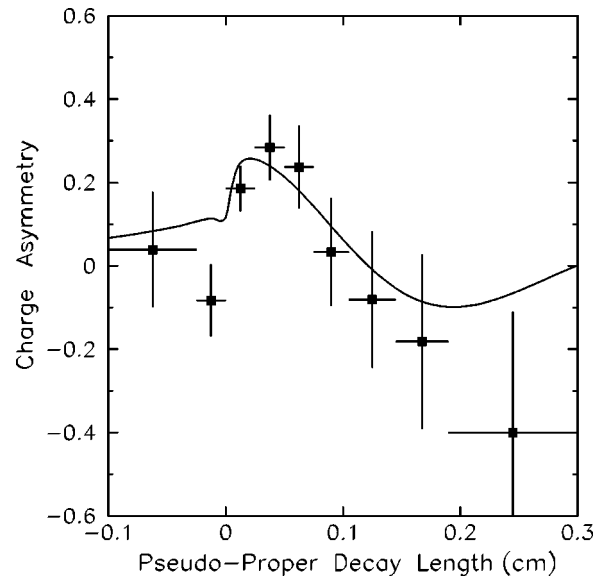| Parameter	Input	Output
Δm_d		0.516 ± 0.099
W		0.325 ± 0.033
f_{BG} $(D^0 \to K^- \pi^+)$	0.227 ± 0.036	0.218 ± 0.030
f_{BG} $(D^0 \to K^- \pi^+ \pi^+ \pi^-)$	0.326 ± 0.040	0.355 ± 0.032
f_{BG} $(D^0 \to K^- \pi^+ \pi^0)$	0.543 ± 0.050	0.489 ± 0.034
f_{SS} $(D^0 \to K^- \pi^+)$	0.487 ± 0.010	0.488 ± 0.010
f_{SS} $(D^0 \to K^- \pi^+ \pi^+ \pi^-)$	0.513 ± 0.007	0.513 ± 0.007
f_{SS} $(D^0 \to K^- \pi^+ \pi^0)$	0.458 ± 0.012	0.465 ± 0.011

FIG. 7. Charge asymmetry of the $l^- D^{*+}$ candidates as a function of pseudo-proper decay length (points). The solid curve shows the result of the Δm_d fit.

TABLE VI. Measurement of Δm_d under various sample composition conditions. Quoted uncertainties are statistical only.

			g^-		Δm_d	
f^{**}	P_V	$\tau(B^-)/\tau(\bar{B}^0)$	$\mu^- D^{*+}$	$e^- D^{*+}$	(ps^{-1})	W
0.24	0.65	1.02	0.121	0.087	0.497 ± 0.093	0.323 ± 0.033
0.36	0.65	1.02	0.187	0.138	0.516 ± 0.099	0.325 ± 0.033
0.48	0.65	1.02	0.263	0.202	0.536 ± 0.108	0.327 ± 0.033
0.36	0.26	1.02	0.090	0.063	0.488 ± 0.090	0.323 ± 0.033
0.36	1.00	1.02	0.250	0.190	0.532 ± 0.106	0.327 ± 0.033
0.36	0.65	0.97	0.179	0.132	0.511 ± 0.098	0.324 ± 0.033
0.36	0.65	1.07	0.194	0.144	0.520 ± 0.101	0.325 ± 0.033

cal only. They are summarized in Table V along with other fit parameters. The fit results are also shown in Fig. 6. The oscillatory behavior can be seen more directly when the asymmetry between the opposite-sign and same-sign events is examined as a function of the pseudo-proper decay length. We define the asymmetry as

$$A(x) = \frac{N^{\text{OS}}(x) - N^{\text{SS}}(x)}{N^{\text{OS}}(x) + N^{\text{SS}}(x)},$$

where $N^{\text{OS}}(x)$ $[N^{\text{SS}}(x)]$ is the number of opposite-sign [same-sign] events. In the ideal case where the backgrounds, the flavor misidentification, and the decay length smearing are absent, the asymmetry is given by $A(x) = \cos(\Delta m_d x/c)$. The asymmetry distribution of the signal sample is illustrated in Fig. 7, together with the fit result.

B. Systematic uncertainties

The sample composition is a source of systematic uncertainty in the oscillation frequency measurement. We have described it in terms of the parameters f^{**}, P_V and the lifetime ratio $\tau(B^-)/\tau(\bar{B}^0)$. We change each one of the parameters to another value while keeping the others at their

TABLE VII. A summary of systematic uncertainties in Δm_d measurement.

	Contribution to	
Source	Δm_d (ps^{-1})	W
Sample composition		
D^{**} fraction (f^{**})	$+0.020$ -0.018	$+0.003$ -0.001
D^{**} composition (P_V)	$+0.017$ -0.027	$+0.002$ -0.001
Lifetime ratio $\tau(B^-)/\tau(\bar{B}^0)$	± 0.005	± 0.001
Physics background	$+0.003$ -0.000	$+0.000$ -0.010
Background shape, $\bar{B}^0$ lifetime	± 0.001	$+0.003$ -0.007
Decay length resolution	± 0.005	$+0.003$ -0.002
B meson momentum estimate	± 0.011	-
Total	$+0.029$ -0.035	$+0.006$ -0.012

nominal values, compute the sample composition g^-, and repeat the fit procedure for Δm_d. We note that the momentum correction factors (K distributions) need to be modified accordingly; the K distributions for the decay $\bar{B} \to l^- \bar{\nu} D^{**}$ have lower mean values because of additional missing particle(s), and changing the amount of D^{**} decays results in changes in the K distributions. The results are summarized in Table VI. We interpret the observed changes as systematic uncertainties.

Other sources of systematic uncertainties considered in this analysis are summarized in Table VII. Physics background processes are studied by adding their simulated decay length distributions to the background function. In addition, the shapes of the decay length distributions of the combinatorial background events and the signal lifetime are subject to uncertainty because they are determined with finite statistical precision. They are changed within uncertainties, and the fit is repeated. We interpret the observed changes as the systematic uncertainty due to this source.

Other sources of systematic uncertainties include our estimates of the decay length resolution and of the B meson momentum. We have introduced a resolution scale factor s and find a value of about 1.2. We change this factor to 1.0 or 1.4 and repeat the fit. We assign the resulting changes as an uncertainty. The B^0 meson momentum estimate (K distribution) is subject to some uncertainty too, because it depends on the kinematics of B meson production and of semileptonic decays. We investigate different production and decay models using the procedure described in Ref. [15], and estimate the uncertainty in the B^0 meson momentum to be 2%, which translates directly to the Δm_d uncertainty.

All contributions are added in quadrature to give the total systematic uncertainty in Δm_d of $^{+0.029}_{-0.035}$ ps^{-1} and in the flavor misidentification probability W of $^{+0.006}_{-0.012}$.

VI. CONCLUSION

We have measured $B^0\bar{B}^0$ mixing using the semileptonic decay $\bar{B}^0 \to l^- \bar{\nu} D^{*+} X$ reconstructed among $\bar{p}p$ collision events with two lepton candidates. The proper decay length is estimated from reconstructed decay vertices and the momentum of the $l^- D^{*+}$ system. A high B^0 purity and a rela-

tively good momentum resolution are achieved. The second lepton candidate in the event is used to infer the flavor of the $\bar{B}^0$ meson at the time of its production, with a flavor misidentification probability of $W = 0.325 \pm 0.033^{+0.006}_{-0.012}$. The frequency of the oscillation is measured to be

$$\Delta m_d = 0.516 \pm 0.099^{+0.029}_{-0.035} \ \text{ps}^{-1},$$

where the first uncertainty is statistical and the second is systematic. The result is consistent with other recent measurements [5–7].

The method could be also applied in the future to a search for $B_s^0 \bar{B}_s^0$ oscillations with a modest value of Δm_s by reconstructing the D_s^+ meson produced in the semileptonic decay $\bar{B}_s^0 \rightarrow l^- \bar{\nu} D_s^+ X$.

ACKNOWLEDGMENTS

[1] ARGUS Collaboration, H. Albrecht *et al.*, Phys. Lett. B **192**, 245 (1987); CLEO Collaboration, M. Artuso *et al.*, Phys. Rev. Lett. **62**, 2233 (1989).

[2] T. Inami and C. S. Lim, Prog. Theor. Phys. **65**, 297 (1981); **65**, 1772(E) (1981).

[3] M. Kobayashi and T. Maskawa, Prog. Theor. Phys. **49**, 652 (1973).

[4] ARGUS Collaboration, H. Albrecht *et al.*, Z. Phys. C **55**, 357 (1992); CLEO Collaboration, J. Bartelt *et al.*, Phys. Rev. Lett. **71**, 1680 (1993); ARGUS Collaboration, H. Albrecht *et al.*, Phys. Lett. B **324**, 249 (1994).

[5] L3 Collaboration, M. Acciarri *et al.*, Eur. Phys. J. C **5**, 195 (1998); DELPHI Collaboration, P. Abreu *et al.*, Z. Phys. C **76**, 579 (1997); OPAL Collaboration, K. Ackerstaff *et al.*, *ibid.* **76**, 417 (1997); ALEPH Collaboration, D. Buskulic *et al.*, *ibid.* **75**, 397 (1997); OPAL Collaboration, G. Alexander *et al.*, *ibid.* **72**, 377 (1996).

[6] OPAL Collaboration, K. Ackerstaff *et al.*, Z. Phys. C **76**, 401 (1997).

[7] CDF Collaboration, F. Abe *et al.*, Phys. Rev. Lett. **80**, 2057 (1998); CDF Collaboration, F. Abe *et al.*, Phys. Rev. D **59**, 032001 (1999); CDF Collaboration, F. Abe *et al.*, *ibid.* **60**, 051101 (1999); CDF Collaboration, F. Abe *et al.*, *ibid.* **60**, 072003 (1999).

[8] ALEPH Collaboration, R. Barate *et al.*, Eur. Phys. J. C **4**, 367 (1998); DELPHI Collaboration, W. Adam *et al.*, Phys. Lett. B **414**, 382 (1997); CDF Collaboration, F. Abe *et al.*, Phys. Rev. Lett. **82**, 3576 (1999).

[9] CDF Collaboration, F. Abe *et al.*, Nucl. Instrum. Methods Phys. Res. A **271**, 387 (1988), and references therein.

[10] D. Amidei *et al.*, Nucl. Instrum. Methods Phys. Res. A **350**, 73 (1994); P. Azzi *et al.*, *ibid.* **360**, 137 (1995).

[11] CDF Collaboration, F. Abe *et al.*, Phys. Rev. D **52**, 2624 (1995).

[12] CDF Collaboration, F. Abe *et al.*, Phys. Rev. Lett. **68**, 2734 (1992); CDF Collaboration, F. Abe *et al.*, Phys. Rev. D **48**, 2998 (1993).

[13] C. Caso *et al.*, Eur. Phys. J. C **3**, 1 (1998).

[14] CDF Collaboration, F. Abe *et al.*, Phys. Rev. Lett. **71**, 3421 (1993); CDF Collaboration, F. Abe *et al.*, Phys. Rev. D **57**, 5382 (1998).

[15] CDF Collaboration, F. Abe *et al.*, Phys. Rev. Lett. **76**, 4462 (1996); CDF Collaboration, F. Abe *et al.*, Phys. Rev. D **58**, 092002 (1998).

[16] CLEO Collaboration, R. Fulton *et al.*, Phys. Rev. D **43**, 651 (1991).

[17] ALEPH Collaboration, D. Busklic *et al.*, Phys. Lett. B **345**, 103 (1995); DELPHI Collaboration, P. Abreu *et al.*, Z. Phys. C **71**, 539 (1996); OPAL Collaboration, R. Akers *et al.*, *ibid.* **67**, 57 (1995); CLEO Collaboration, Phys. Rev. Lett. **80**, 4127 (1998).

[18] N. Isgur, D. Scora, B. Grinstein, and M. Wise, Phys. Rev. D **39**, 799 (1989); D. Scora and N. Isgur, *ibid.* **52**, 2783 (1995).

[19] R. M. Barnett *et al.*, Phys. Rev. D **54**, 1 (1996).

[20] P. Nason, S. Dawson, and R. K. Ellis, Nucl. Phys. **B327**, 49 (1989); **B335**, 260(E) (1990).

[21] C. Peterson, D. Schlatter, I. Schmitt, and P. M. Zerwas, Phys. Rev. D **27**, 105 (1983).

[22] P. Avery, K. Read, and G. Trahern, Report No. CSN-212, 1985.

[23] ALEPH Collaboration, D. Buskulic *et al.*, Phys. Lett. B **377**, 205 (1996).